

# Real-Time Detection of Reverse-Osmosis Membrane Scaling via Raman Spectroscopy

Omkar D. Supekar,<sup>†,||</sup> Joseph J. Brown,<sup>†,||,∇</sup> Alan R. Greenberg,<sup>\*,†,||</sup> Juliet T. Gopinath,<sup>‡,§,||</sup> and Victor M. Bright<sup>†,||</sup>

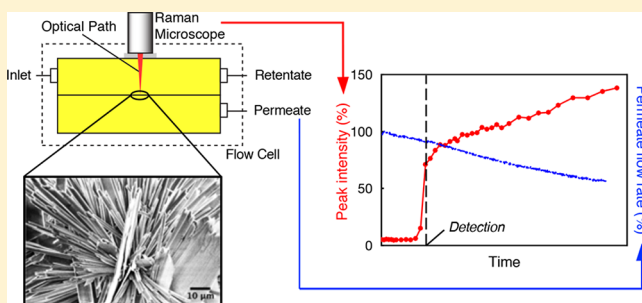
<sup>†</sup>Department of Mechanical Engineering, University of Colorado, Boulder, Colorado 80309, United States

<sup>‡</sup>Department of Electrical, Computer, and Energy Engineering, University of Colorado, Boulder, Colorado 80309, United States

<sup>§</sup>Department of Physics, University of Colorado, Boulder, Colorado 80309, United States

<sup>||</sup>Membrane Science, Engineering and Technology Center, University of Colorado, Boulder, Colorado 80309, United States

**ABSTRACT:** Scaling remains a serious barrier to membrane-based desalination. While some real-time techniques have proven effective for scaling detection, none provides the crucial capability of chemical identification with high temporal and spatial resolution under realistic operating conditions. In this work, we describe a real-time technique for detection of early stage scaling via chemical quantification using Raman spectroscopy. Experiments utilized a custom bench-scale flow cell integrated with a commercial Raman microscope that accesses the membrane through a 10 mm optical window. Calcium sulfate was used as a model foulant at high concentration (1.8 g/L) to minimize the time required for membrane scaling. The experiments were conducted with a commercial brackish water reverse-osmosis thin film composite membrane operating at a feed pressure of 1.17 MPa (170 psi) and a feed flow velocity of 4.7–5.6 cm/s. Raman measurements were made in real time at a laser excitation wavelength of 785 nm. Real-time results were validated with post-mortem SEM and energy-dispersive X-ray analysis and indicated the capability to detect early-stage scaling characterized by a relatively modest reduction in the permeate flow rate.



## 1. INTRODUCTION

Membranes are essential components in many industrial separation applications. However, a major challenge in their use is membrane fouling, which can lead to an increase in operating pressure and/or a decrease in flow rate, resulting in higher energy consumption and operating costs. While pressure and permeate flow are typically monitored during operation to indicate the development of fouling, these metrics provide limited information on the location or chemistry of the foulants. In membrane-based desalination, concentration polarization<sup>1–3</sup> usually induces a spatial dependence on the onset and growth of inorganic fouling (scaling) necessitating a real-time, local monitoring technique for optimum scaling detection. One solution is offered by ultrasonic reflectometry (UR),<sup>4–9</sup> which has been used in conjunction with flow reversal techniques to mitigate the development of scaling during desalination.<sup>7,8</sup> However, UR provides no chemical information on the foulants. Similarly, many direct observation techniques<sup>10,11</sup> also lack the capability of providing chemical identification. Other noninvasive fouling detection methods reported in the literature include magnetic resonance imaging,<sup>12,13</sup> X-ray micro imaging,<sup>14</sup> electrical impedance spectrometry,<sup>15,16</sup> and streaming potential measurement.<sup>17</sup> However, these methods generally have low spatial and/or temporal resolution, require expensive detection equipment,

and/or are limited by the foulants that can be chemically detected. In contrast, Raman spectroscopy offers a viable alternative with diffraction-limited spatial resolution, chemical quantification of the foulants, and the potential to provide early-stage scaling detection.

Raman spectroscopy is a technique used to identify the chemical fingerprint of a sample with inelastic scattering from optical phonons. The energy difference between the incident and scattered photons is used to characterize vibrational modes in the chemical bonds of a substrate for its chemical identification.<sup>18</sup> In previous work, Raman spectroscopy has been used as a technique for off-line chemical characterization of membrane structures and organic fouling.<sup>18–23</sup> The use of metal nanostructures within the membrane structure enhances the Raman signal (surface-enhanced Raman spectroscopy, SERS) from the membrane and foulant, and has been used for real-time biofouling monitoring in nanofiltration.<sup>24,25</sup> However, SERS cannot easily be adapted for large-scale separation processes. While conventional Raman spectroscopy

**Special Issue:** Richard Noble Festschrift

**Received:** March 22, 2018

**Revised:** May 24, 2018

**Accepted:** May 24, 2018

**Published:** May 24, 2018

has been recently demonstrated for detecting and monitoring adsorption of an organic foulant on ultrafiltration membranes,<sup>26</sup> this study is the first to report real-time detection of inorganic foulants under realistic operating conditions.

In this initial study, we report the use of Raman spectroscopy for the real-time detection of membrane scaling during reverse osmosis (RO) desalination. In particular, the experiments demonstrate the capability of detecting early-stage scaling, corresponding to a permeate flow-rate reduction of only ~3%–11%. The work utilized a custom-designed bench-scale flat sheet flow cell with an integrated microscope objective and optical window for laser access. The experiments were conducted under realistic operating conditions, using calcium sulfate dihydrate ( $\text{CaSO}_4 \cdot 2\text{H}_2\text{O}$ ) as a model scalant at a sufficiently high feed concentration to expedite the onset of scaling. Scaling was determined by monitoring the changes in the relative intensity of Raman peaks associated with calcium sulfate. Initial results suggest that Raman spectroscopy offers the potential for effective real-time chemical identification of early-stage membrane scaling.

## 2. MATERIALS AND METHODS

**2.1. Bench-Scale Cross-Flow RO System.** A custom bench-scale separation system integrated with Raman spectroscopy capability was designed and fabricated. This small footprint system is shown in Figure 1. The system contains

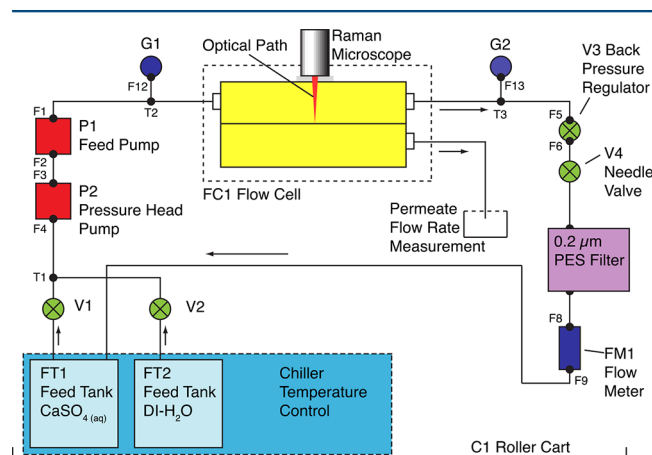


**Figure 1.** Diagram of flow cell instrumentation for the scaling experiments. [Legend: G#, gauges; F#, fittings; V#, valves; and T#, T-fittings.]

two 9-L tanks: one for deionized (DI) water and the other for the aqueous salt solution. The temperature for the feed solutions was controlled at  $24 \pm 1$  °C, using a stainless steel heat exchanger connected to a chiller (Model CFT-25, Thermo Neslab). An inline pressure head pump (Model 3-MD-SC, Little Giant Franklin Electric) is connected to the feed tanks in order to eliminate possible cavitation in the high-pressure pump. The pressure head pump is connected to a rotary vane pump (Model TMRSS051A, Fluid-o-Tech) to provide feed flow at the desired pressure. A backpressure regulator (Model 12-251B2-4AZ5, Neon) and a needle valve (Model SS-1RS4, Swagelok) were installed at the outlet of the flow cell. Two pressure gauges were located upstream and downstream of the flow cell to monitor the inlet pressure and the pressure drop across the flow cell. A flow meter (Model 74C-234G041-421330, King) was connected on the retentate line to monitor

the flow through the RO system. An inline filter (Model CCS-020-C1B, 0.2  $\mu\text{m}$ , Advantec) is installed downstream of the flow cell on the retentate line to filter particulates from the feed. Retentate from the flow cell is returned to the feed tank, and the permeate flow is collected in a glass beaker placed on a precision balance (Model PNX-2002, American Weigh Scales). The computer-connected balance records the permeate flow rate at 1 min intervals.

The flat-sheet stainless-steel membrane flow cell has a top component with a 100 mm long rectangular flow channel (50 mm wide  $\times$  2 mm thick) with a cross-sectional area of  $1.00 \times 10^{-4}$  m<sup>2</sup>. The top component contains the feed inlet port, retentate outlet port, and a cavity that accommodates a 25.4 mm-diameter optical window (1.5 mm thick), providing optical access to the flow cell for Raman spectroscopy via a 10 mm hole in the center of the flow channel. The optical window is placed in the cavity and sealed with an O-ring using a clamp, which accommodates the microscope objective. The bottom component contains the permeate outlet port, as well as a stainless-steel mesh to support the membrane. The two components are sealed using a double O-ring arrangement to ensure operation at the required pressure. A detailed schematic of the flow cell design and its components is shown in Figure 2.

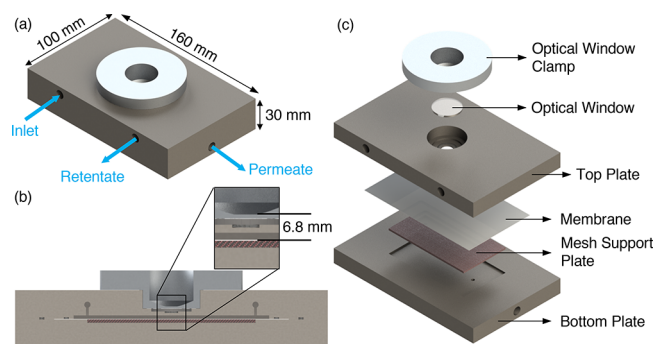


**Figure 2.** (a) Schematic of the assembled flow cell. (b) Sectional side view showing a 7.5-mm spacing between the optical access port and the membrane. (c) Exploded view.

Prior to the start of each experiment, the flow cell was cleaned with isopropanol and DI water, and the RO system was flushed with DI water for 1 h. The membrane used in the experiments was a commercially available brackish water polyamide membrane UTC-73HA (Toray). The membrane was cut to appropriate dimensions (115 mm  $\times$  65 mm), soaked in a 50% aqueous isopropanol solution for 20 min, and then inserted into the flow cell. Scaling experiments were conducted at a pressure of 1.17 MPa (170 psi) at a flow rate of 17–20 L/h (4.7–5.6 cm/s). For the first part of the experiment, the system was operated with deionized (DI) water at pressure for at least 12 h to compact the membrane. Once a steady-state flow was achieved, the feed was switched to a calcium sulfate dihydrate (99% Reagent Plus, Sigma–Aldrich) aqueous solution with a concentration of 1.8 g/L. A high concentration of calcium sulfate was chosen to expedite the onset of scaling and decrease the time required for the run. Real-time Raman spectral acquisition was maintained during the experiment.

**2.2. Integration of Raman Microscope with the Flow Cell.** Real-time Raman spectroscopy was conducted using a commercial confocal Raman microscope (model inVia Reflex, Renishaw). The microscope objective (Model N-PLAN L50X, Leica; working distance of 8.2 mm) was integrated with the

flow cell through the optical window for access to the center of the flow cell. A 785 nm continuous wave (cw) laser (Model I0785SD0090B-IS, Innovative Photonic Solutions) was used as the excitation source. The laser power from the objective was measured to be  $\sim 20$  mW. The flow cell was mounted on a high-load-capacity vertical translation stage (Model VAP4, Thorlabs), which enables the laser to be focused onto the membrane precisely and fix the focus spot with minimum vertical drift over the course of the experiment. The objective focuses the beam to a spot of  $\sim 3$   $\mu\text{m}$  (full width, half maximum) on the focal plane. Spectral acquisition was performed every 5 min until a prominent calcium sulfate Raman peak was observed, and every 10 min thereafter. The acquired spectra contain the Raman peaks and broadband background fluorescence from the membrane. The fluorescence signal is removed from the spectrum, using the baseline removal tool in the Raman microscope software (WiRe 4.4). The signal was then normalized to the most prominent peak intensity of the membrane spectrum near  $1150$   $\text{cm}^{-1}$ . The Raman signature of calcium sulfate has prominent peaks at 495, 1008, and  $1134$   $\text{cm}^{-1}$ .<sup>27</sup> The presence of scaling during the experiment was confirmed by monitoring the ratio of the strongest calcium sulfate Raman peak at  $1008$   $\text{cm}^{-1}$  (from ref 27) and the most prominent membrane peak at  $1150$   $\text{cm}^{-1}$ .

**2.3. Post-Mortem Characterization.** Upon completion of each experiment, the flow cell was drained, and the membrane then removed and dried under ambient conditions for at least 24 h. The membrane was sectioned to an area of  $\sim 5$   $\text{cm}^2$  around the center of the membrane for scanning electron microscopy (SEM) (Model JSM 6480-LV, JEOL) and energy-dispersive X-ray (EDX) analysis (Model Noran System SIX, ThermoFisher Scientific). Image morphology and corresponding elemental analysis provided confirmation of membrane scaling.<sup>28</sup>

### 3. RESULTS AND DISCUSSION

This initial study consisted of four independent experiments. The first of these continued until the permeate flow rate decreased by  $\sim 40\%$ . Three additional experiments were conducted as a time series for which the total run time was systematically varied in order to capture different degrees of scaling in the region interrogated by the sensor. The results are summarized in Table 1 and are arranged in order of decreasing Raman detection time. The data provide a basis for estimating the real-time Raman detection limit during early stage scaling. The experiments were performed under identical initial operating conditions (pressure, feed flow rate, and temper-

ature), but as expected, reflected variability typical for membrane scaling studies.<sup>9</sup> Nevertheless, the data from each experiment indicate a similar relationship between the real-time and post-mortem metrics.

Test 1 was conducted for 8 h, during which time the permeate flow rate decreased by  $\sim 42\%$  during operation with the calcium sulfate feed solution. The initial Raman spectrum obtained during the DI water phase reflects the peaks corresponding to the bonds that characterize the polyamide membrane; subsequently, after switching to the salt solution feed, calcium sulfate peaks at  $495$  and  $1008$   $\text{cm}^{-1}$  (from ref 27) appear and increase in magnitude through the end of the experiment (see Figure 3a).

Figure 3b shows the change in permeate flow rate with time and the corresponding response of the relative calcium sulfate Raman peak intensity ( $1008$   $\text{cm}^{-1}$ ). Here, the initial sharp rise in Raman intensity beginning at  $\sim 80$  min extends through  $\sim 100$  min and then transitions to a continued monotonic increase at a relatively constant but distinctly lower rate. During exposure to the calcium sulfate feed solution, the relative peak intensity increases by  $\sim 140\%$ . By comparison, the permeate flow rate decreases at an approximately constant rate for a total decrease of  $\sim 42\%$  through the end of the experiment.

To confirm that the real-time results were due to scaling, post-mortem analysis of the membrane was conducted. Representative low- and higher-magnification SEM images are shown in Figures 4a and 4b. The former indicates extensive coverage of the membrane surface while the latter clearly shows the rosette morphology typical of calcium sulfate scaling.<sup>9,28</sup> X-ray analysis (Figure 4c) identifies the fouling layer as calcium sulfate.

Two time-series tests (2a and 2b, Table 1) were performed to confirm the results obtained for test 1, as well as to explore early-stage scaling detection capabilities. These tests were initiated with predetermined durations of 90 min (test 2a) and 65 min (test 2b), based on results from test 1. These durations corresponded to increases in peak intensity of  $\sim 100\%$  and  $\sim 150\%$ , compared with decreases in the permeate flow rate of  $\sim 9$  and  $\sim 25\%$ , respectively. Despite some variability in the permeate flow rates, increases in Raman relative peak intensity provided overall real-time characteristics similar to those observed in test 1. SEM and EDX post-mortem results similarly resembled those in Figure 4.

A third time-series experiment was conducted such that the test was halted within a few minutes of the initial Raman peak increase so that post-mortem analysis could be conducted close to initial detection. The permeate flow rate and Raman relative peak intensity are shown as a function of time in Figure 5a. The responses are again similar to those in the other experiments. Here, the increase in peak intensity occurs after  $\sim 20$  min, at which time the permeate flow rate has decreased by  $\sim 4\%$ . It is important to note that the Raman sensing used here is a point measurement such that the response reflects scaling in only a small area ( $\sim 7$   $\mu\text{m}^2$ ). Thus, the time at which scaling is first detected is dependent on the locally random nature of initial precipitation in the region around the target coordinates. The post-mortem results presented in Figure 5b are from the area that encompassed the target coordinates, and confirm the potential of Raman spectroscopy for early-stage scaling detection.

The overall decrease in permeate flow rate during flow cell operation can be reasonably attributed to membrane compaction, in addition to scaling.<sup>29</sup> The magnitude of

**Table 1. Summary Metrics for the Four Independent Experiments<sup>b</sup>**

test	total run time (min)	initial permeate flow rate <sup>a</sup> (mL/min)	net permeate flow rate reduction <sup>a</sup> (%)	time for CaSO <sub>4</sub> Raman peak detection <sup>a,b</sup> (min)	permeate flow rate reduction at Raman detection <sup>a</sup> (%)
1	480	4.6	42.4	90	8.5
2a	86	4.7	9.4	45	3.2
2b	65	5.5	24.7	30	8.2
3	28	5.4	7.8	25	11.3

<sup>a</sup>Values obtained during operation with calcium sulfate feed solution.

<sup>b</sup>The time for Raman peak detection is defined as that taken to detect a relative CaSO<sub>4</sub> peak above 50%.

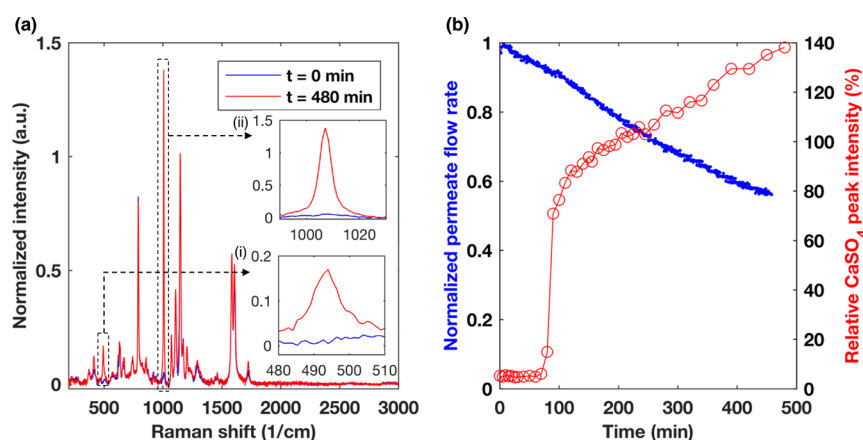


**Figure 3.** (a) Comparison of Raman spectra at the beginning (blue) and at the end (red) of test 1. The Raman peaks corresponding to calcium sulfate at (i)  $495\text{ cm}^{-1}$  and (ii)  $1008\text{ cm}^{-1}$  increased in magnitude relative to those from the membrane. (b) Comparison of the normalized permeate flow rate and Raman  $1008\text{ cm}^{-1}$  peak intensity; the distinct increase in the Raman peak intensity corresponds to a permeate flow rate decrease of  $\sim 9\%$ .

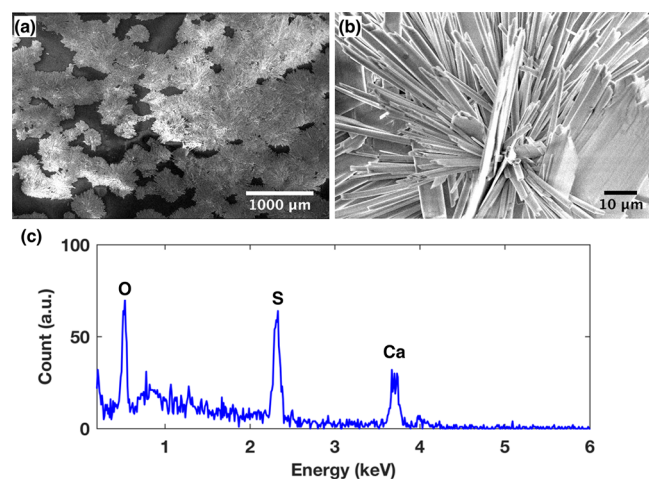


**Figure 4.** (a) Low-magnification and (b) higher-magnification SEM images of the membrane surface, indicating extensive surface coverage and the rosette morphology characteristic of calcium sulfate scaling. (c) Scaling has been identified as calcium sulfate via energy-dispersive X-ray analysis.

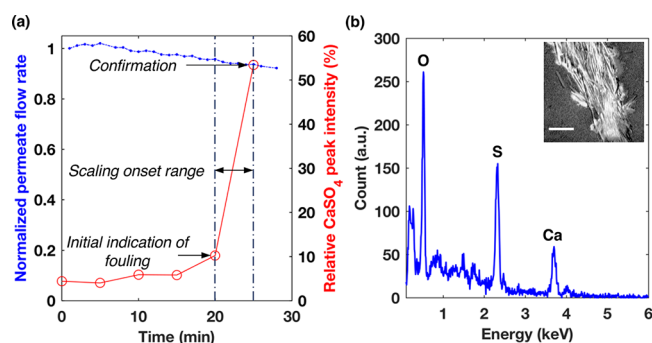


**Figure 5.** Real-time and post-mortem results from test 3, halted at 28 min: (a) permeate flow rate and relative ( $1008\text{ cm}^{-1}$ ) peak intensity and (b) energy-dispersive X-ray analysis from the region beneath the microscope objective with a corresponding SEM image shown in the inset (scale bar =  $20\text{ }\mu\text{m}$ ).

compaction is dependent on membrane mechanical and structural characteristics, as well as operational parameters such as pressure. An important advantage of Raman spectroscopy

copy,<sup>16</sup> as well as other real-time detection techniques, such as ultrasonic reflectometry,<sup>4</sup> electrical impedance spectroscopy,<sup>16</sup> and direct optical imaging<sup>11</sup> is that they respond to scaling rather than compaction. However, of these techniques, only Raman spectroscopy has the capability to distinguish and chemically quantify the scalants.

The results from the four independent experiments demonstrate the potential of real-time, Raman-based detection of membrane scaling under realistic operating conditions. In each case, the data clearly show a similar inverse relationship between peak intensity and permeate flow rate with the change in the former more pronounced than the decrease in the latter. A limitation of the study is that peak intensity particularly in early-stage scaling is dependent on the random occurrence of scaling initiation at only one set of target coordinates. This could be addressed by increasing the sensing area by deploying multiple sensors or employing more-sophisticated techniques, such as laser scanning confocal Raman microscopy.<sup>30</sup> In addition, appropriate caution is warranted, given the small sample size employed in these preliminary tests. A more comprehensive set of replicated experiments is currently underway in which feed composition and concentration are systematically varied.

## 4. CONCLUSIONS

Real-time bench-scale RO-membrane scaling experiments employing Raman spectroscopy showed a consistent inverse relationship between the permeate flow rate and calcium sulfate peak intensity. The significant increase in Raman peak intensity during the experiments was due to calcium sulfate scaling, as confirmed by post-mortem analysis. To the best of our knowledge, this work is the first to demonstrate the real-time scaling detection capability of Raman spectroscopy under realistic operating conditions. An important consequence of this work is that identification of scalant chemistry during membrane operation could lead to improved fouling remediation measures.

## AUTHOR INFORMATION

### Corresponding Author

\*E-mail: alan.greenberg@colorado.edu.

ORCID 

Omkar D. Supekar: 0000-0003-1777-8508

Alan R. Greenberg: 0000-0003-1785-9439

## Present Address

<sup>∇</sup>Current affiliation: Department of Mechanical Engineering, University of Hawai'i at Mānoa, Honolulu, HI 96822.

## Notes

The authors declare no competing financial interest.

## ACKNOWLEDGMENTS

The authors gratefully acknowledge support of this work by the Membrane Science, Engineering and Technology (MAST) Center, and the technical insights provided by Dr. Joseph Swisher and Dr. Abhoyjit Bhowan, from Electrical Power Research Institute (EPRI). The authors appreciate the invaluable machining assistance provided by Dragan Mejic in the Department of Chemical and Biological Engineering instrument shop, technical assistance by Masoud Aghajani and Dr. Ozge Heinz in the Department of Mechanical Engineering, and Dr. Mo Zohrabi in the Department of Electrical, Computer and Energy Engineering at the University of Colorado–Boulder. The authors are grateful to Prof. Virginia Ferguson in the Department of Mechanical Engineering at the University of Colorado–Boulder for access to the Raman microscope system.

## REFERENCES

- (1) Prabhakar, S.; Ramani, M. P. S. A New Concept of Mass Transfer Coefficient in Reverse Osmosis—Practical Applications. *J. Membr. Sci.* **1994**, *86* (1–2), 145–154.
- (2) Sutzkover, I.; Hasson, D.; Semiat, R. Simple Technique for Measuring the Concentration Polarization Level in a Reverse Osmosis System. *Desalination* **2000**, *131* (1–3), 117–127.
- (3) Sobana, S.; Panda, R. C. Identification, Modelling, and Control of Continuous Reverse Osmosis Desalination System: A Review. *Sep. Sci. Technol.* **2011**, *46* (4), 551–560.
- (4) Mairal, A. P.; Greenberg, A. R.; Krantz, W. B.; Bond, L. J. Real-Time Measurement of Inorganic Fouling of RO Desalination Membranes Using Ultrasonic Time-Domain Reflectometry. *J. Membr. Sci.* **1999**, *159* (1–2), 185–196.
- (5) Sanderson, R. D.; Li, J.; Hallbauer, D. K.; Sikder, S. K. Fourier Wavelets from Ultrasonic Spectra: A New Approach for Detecting the Onset of Fouling during Microfiltration of Paper Mill Effluent. *Environ. Sci. Technol.* **2005**, *39* (18), 7299–7305.
- (6) Cobry, K. D.; Yuan, Z.; Gilron, J.; Bright, V. M.; Krantz, W. B.; Greenberg, A. R. Comprehensive Experimental Studies of Early-Stage Membrane Scaling during Nanofiltration. *Desalination* **2011**, *283*, 40–51.
- (7) Lu, X.; Kujundzic, E.; Mizrahi, G.; Wang, J.; Cobry, K.; Peterson, M.; Gilron, J.; Greenberg, A. R. Ultrasonic Sensor Control of Flow Reversal in RO Desalination—Part 1: Mitigation of Calcium Sulfate Scaling. *J. Membr. Sci.* **2012**, *419–420*, 20–32.
- (8) Mizrahi, G.; Wong, K.; Lu, X.; Kujundzic, E.; Greenberg, A. R.; Gilron, J. Ultrasonic Sensor Control of Flow Reversal in RO Desalination. Part 2: Mitigation of Calcium Carbonate Scaling. *J. Membr. Sci.* **2012**, *419–420*, 9–19.
- (9) Kujundzic, E.; Greenberg, A. R.; Peterson, M. Review: Ultrasonic Characterization of Membranes. *Desalin. Water Treat.* **2014**, *52* (7–9), 1217–1249.
- (10) Le-Clech, P.; Marselina, Y.; Ye, Y.; Stuetz, R. M.; Chen, V. Visualisation of Polysaccharide Fouling on Microporous Membrane Using Different Characterisation Techniques. *J. Membr. Sci.* **2007**, *290* (1–2), 36–45.
- (11) Bartman, A. R.; Lyster, E.; Rallo, R.; Christofides, P. D.; Cohen, Y. Mineral Scale Monitoring for Reverse Osmosis Desalination via Real-Time Membrane Surface Image Analysis. *Desalination* **2011**, *273* (1), 64–71.
- (12) Buetehorn, S.; Utiu, L.; Küppers, M.; Blümich, B.; Wintgens, T.; Wessling, M.; Melin, T. NMR Imaging of Local Cumulative Permeate Flux and Local Cake Growth in Submerged Microfiltration Processes. *J. Membr. Sci.* **2011**, *371* (1–2), 52–64.
- (13) Li, X.; Mo, Y.; Li, J.; Guo, W.; Ngo, H. H. In-Situ Monitoring Techniques for Membrane Fouling and Local Filtration Characteristics in Hollow Fiber Membrane Processes: A Critical Review. *J. Membr. Sci.* **2017**, *528*, 187–200.
- (14) Yeo, A.; Yang, P.; Fane, A. G.; White, T.; Moser, H. O. Non-Invasive Observation of External and Internal Deposition during Membrane Filtration by X-ray Microimaging (XMI). *J. Membr. Sci.* **2005**, *250* (1–2), 189–193.
- (15) Antony, A.; Chilcott, T.; Coster, H.; Leslie, G. In Situ Structural and Functional Characterization of Reverse Osmosis Membranes Using Electrical Impedance Spectroscopy. *J. Membr. Sci.* **2013**, *425–426*, 89–97.
- (16) Hu, Z.; Antony, A.; Leslie, G.; Le-Clech, P. Real-Time Monitoring of Scale Formation in Reverse Osmosis Using Electrical Impedance Spectroscopy. *J. Membr. Sci.* **2014**, *453*, 320–327.
- (17) Chun, M. S.; Il Cho, H.; Song, I. K. Electrokinetic Behavior of Membrane Zeta Potential during the Filtration of Colloidal Suspensions. *Desalination* **2002**, *148* (1–3), 363–367.
- (18) Goh, P. S.; Ismail, A. F.; Ng, B. C. Raman Spectroscopy. *Forensics Libr.* **2017**, 31–46.
- (19) Cui, L.; Yao, M.; Ren, B.; Zhang, K. S. Sensitive and Versatile Detection of the Fouling Process and Fouling Propensity of Proteins on Polyvinylidene Fluoride Membranes via Surface-Enhanced Raman Spectroscopy. *Anal. Chem.* **2011**, *83* (5), 1709–1716.
- (20) Khulbe, K. C.; Matsuura, T. Characterization of Synthetic Membranes by Raman Spectroscopy, Electron Spin Resonance, and Atomic Force Microscopy: A Review. *Polymer* **2000**, *41* (5), 1917–1935.
- (21) Lamsal, R.; Harroun, S. G.; Brosseau, C. L.; Gagnon, G. A. Use of Surface Enhanced Raman Spectroscopy for Studying Fouling on Nanofiltration Membrane. *Sep. Purif. Technol.* **2012**, *96*, 7–11.
- (22) Khulbe, K. C.; Gagné, S.; Tabe Mohammadi, A.; Matsuura, T.; Lamarche, A. M. Investigation of Polymer Morphology of Integral-Asymmetric Membranes by ESR and Raman Spectroscopy and Its Comparison with Homogeneous Films. *J. Membr. Sci.* **1995**, *98* (3), 201–208.
- (23) Dodda, J. M.; Bělský, P.; Chmelář, J.; Remiš, T.; Smolná, K.; Tomáš, M.; Kullová, L.; Kadlec, J. Comparative Study of PVA/SiO<sub>2</sub> and PVA/SiO<sub>2</sub>/glutaraldehyde (GA) Nanocomposite Membranes Prepared by Single-Step Solution Casting Method. *J. Mater. Sci.* **2015**, *50* (19), 6477–6490.
- (24) Kögler, M.; Zhang, B.; Cui, L.; Shi, Y.; Yliperttula, M.; Laaksonen, T.; Viitala, T.; Zhang, K. Real-Time Raman Based Approach for Identification of Biofouling. *Sens. Actuators, B* **2016**, *230*, 411–421.
- (25) Chao, Y.; Zhang, T. Surface-Enhanced Raman Scattering (SERS) Revealing Chemical Variation during Biofilm Formation: From Initial Attachment to Mature Biofilm. *Anal. Bioanal. Chem.* **2012**, *404* (5), 1465–1475.
- (26) Virtanen, T.; Reinikainen, S. P.; Kögler, M.; Mänttari, M.; Viitala, T.; Kallioinen, M. Real-Time Fouling Monitoring with Raman Spectroscopy. *J. Membr. Sci.* **2017**, *525*, 312–319.
- (27) Prieto-Taboada, N.; Gómez-Laserna, O.; Martínez-Arkarazo, I.; Olazabal, M. Á.; Madariaga, J. M. Raman Spectra of the Different Phases in the CaSO<sub>4</sub>–H<sub>2</sub>O System. *Anal. Chem.* **2014**, *86* (20), 10131–10137.
- (28) Shih, W.-Y.; Rahardianto, A.; Lee, R.-W.; Cohen, Y. Morphometric Characterization of Calcium Sulfate Dihydrate (Gypsum) Scale on Reverse Osmosis Membranes. *J. Membr. Sci.* **2005**, *252* (1–2), 253–263.
- (29) Aghajani, M.; Maruf, S. H.; Wang, M.; Yoshimura, J.; Pichorim, G.; Greenberg, A.; Ding, Y. Relationship between Permeation and

Deformation for Porous Membranes. *J. Membr. Sci.* **2017**, *S26*, 293–300.

(30) Patil, C. A.; Arrasmith, C. L.; Mackanos, M. A.; Dickensheets, D. L.; Mahadevan-Jansen, A. A Handheld Laser Scanning Confocal Reflectance Imaging-Confocal Raman Microspectroscopy System. *Biomed. Opt. Express* **2012**, *3* (3), 488.